Programmable Interference between Two Microwave Quantum Memories

Yvonne Y. Gao,[1,*] Brian J. Lester,[1] Yaxing Zhang,[1] Chen Wang,[2] Serge Rosenblum,[1] Luigi Frunzio,[1] Liang Jiang,[1] S. M. Girvin,[1] and Robert J. Schoelkopf[1,†]

[1]*Departments of Physics and Applied Physics, Yale University, New Haven, Connecticut 06520, USA and Yale Quantum Institute, Yale University, New Haven, Connecticut 06511, USA*
[2]*University of Massachusetts, Amherst, Massachusetts 01003-9337, USA*

(Received 23 February 2018; revised manuscript received 27 April 2018; published 21 June 2018)

Interference experiments provide a simple yet powerful tool to unravel fundamental features of quantum physics. Here we engineer a driven, time-dependent bilinear coupling that can be tuned to implement a robust 50:50 beam splitter between stationary states stored in two superconducting cavities in a three-dimensional architecture. With this, we realize high-contrast Hong-Ou-Mandel interference between two spectrally detuned stationary modes. We demonstrate that this coupling provides an efficient method for measuring the quantum state overlap between arbitrary states of the two cavities. Finally, we showcase concatenated beam splitters and differential phase shifters to implement cascaded Mach-Zehnder interferometers, which can control the signature of the two-photon interference on demand. Our results pave the way toward implementation of scalable boson sampling, the application of linear optical quantum computing protocols in the microwave domain, and quantum algorithms between long-lived bosonic memories.

DOI: 10.1103/PhysRevX.8.021073 Subject Areas: Quantum Physics

I. INTRODUCTION

Interference experiments are one of the simplest probes into many of the riveting facets of quantum mechanics, from wave-particle duality to nonclassical correlations. The seminal work by Hong, Ou, and Mandel (HOM) is an elegant manifestation of two-particle quantum interference arising from bosonic quantum statistics [1]. In their experiment, two photons incident on a 50:50 beam splitter (BS) always exit in pairs from the same, albeit random, output port. Central to such interference experiments is the unitary operation $\hat{U}_{\mathrm{BS}} = \exp[i(\pi/4)(\hat{a}\hat{b}^{\dagger} + \hat{a}^{\dagger}\hat{b})]$. For propagating particles, this is simply realized with a 50:50 beam splitter, but more generally, it can be implemented by engineering a time-dependent coupling of the form $\hat{H}_{\mathrm{int}}(t)/\hbar = g(t)\hat{a}\hat{b}^{\dagger} + g^{*}(t)\hat{a}^{\dagger}\hat{b}$. Recent experiments have demonstrated this type of coupling in different physical systems, enabling interference of both bosonic and fermionic particles [2–5]. These results have shed light on the concept of entanglement [6,7] and enabled fundamental tests of quantum mechanics like the violation of Bell's inequalities [8]. They also have profound technological implications, with new applications in areas such as quantum metrology [9], simulation [10], and information processing [11,12].

Superconducting systems have been proposed as a promising platform to study bosonic interference and implement scalable boson sampling [13]. In particular, superconducting microwave cavities coupled to transmons or other nonlinear ancillas in the circuit quantum electrodynamics (cQED) framework have the capability to deterministically create complex bosonic states [14,15] and perform robust measurements of photon statistics. So far, interference between harmonic oscillator modes has been demonstrated in cQED systems using elements with tunable frequencies [16–19]. However, such systems tend to suffer from unfavorable coherence properties, limiting the complexity of the experiment to single photons. Recently it has been shown that three-dimensional, fixed-frequency superconducting microwave cavities have excellent coherence properties [20,21], making them attractive quantum memories. We can also readily prepare and manipulate complex quantum states in these cavities using the transmon as an ancilla. However, direct interference between bosonic states stored in these memories has remained a challenge due to the complexity of realizing high-quality beam splitters and differential phase shifters (DPS) between stationary quantum memory modes.

In this work, we showcase the on-demand interference of stationary bosonic modes stored in two spectrally separated, long-lived superconducting microwave cavities,

*Corresponding author.
yvonne.gao@yale.edu
†Corresponding author.
robert.schoelkopf@yale.edu

Alice and Bob. Our implementation employs a frequency-converting bilinear coupling between them which can be programmed to effectively implement a robust BS. With this capability, we demonstrate HOM interference between the two memories with a contrast up to 98% ± 1%. Further, we combine this with photon-number parity measurement to perform efficient determination of quantum state overlap [7,22]. Lastly, we demonstrate *in situ* manipulation of two-photon interference through cascaded Mach-Zehnder (MZ) interferometers constructed with multiple BS and DPS. This highlights the versatility of our implementation and opens the door to more complex interference experiments in cQED.

II. IMPLEMENTATION AND CHARACTERIZATION

Stationary photons stored in the two spectrally separated cavities can interfere only if their energies are made indistinguishable. To do so, we can engineer a direct, tunable bilinear coupling $\hat{H}_{\rm int}$ between Alice and Bob, whose resonance frequencies ω_a and ω_b are separated by ∼1 GHz to ensure minimal residual coupling [23]. The effective circuit of the system is depicted in Fig. 1(a). The transmon ancilla, qA, couples only to Alice to provide the capability of fast single-cavity manipulations. The Y-shaped transmon [24], qC, weakly couples dispersively to both Alice and Bob. Its single Josephson junction provides the necessary nonlinearity to activate the desired bilinear coupling through four-wave mixing in the presence of the appropriate drives. The Hamiltonian of the Josephson

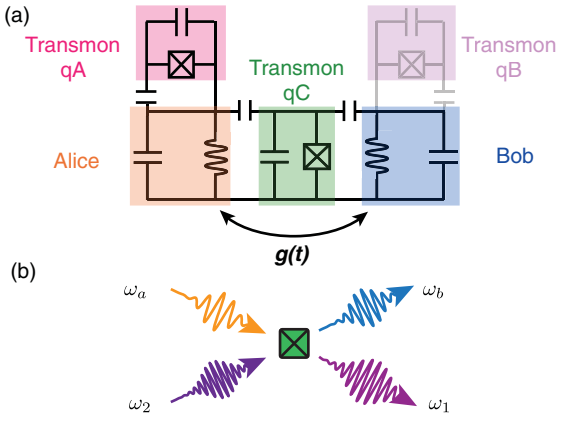

FIG. 1. cQED system. (a) The effective circuit of the cQED system containing two high-Q harmonic oscillators (orange, blue) bridged by a transmon (green), as well as an additional transmon mode (pink) that only capacitively couples to Alice. A similar ancillary transmon (purple) can also be used, but it is not necessary for this experiment. The resonance frequency of Alice and Bob are detuned from each other by ∼1 GHz to minimize undesired cross talk. (b) Four-wave mixing process through the Josephson junction of qC that enables the bilinear coupling between Alice and Bob when $\omega_2 - \omega_1 = \omega_b - \omega_a$.

junction in the presence of two drives, with frequencies ω_1 and ω_2 and normalized amplitudes ξ_1 and ξ_2, is given by [25,26]

$$\hat{H} = -E_J \cos\left[\phi_a(\hat{a} + \hat{a}^\dagger) + \phi_b(\hat{b} + \hat{b}^\dagger) + \phi_c(\hat{c} + \hat{c}^\dagger + \xi_1 + \xi_1^* + \xi_2 + \xi_2^*)\right], \quad (1)$$

where $\hat{a}$ and $\hat{b}$ are the creation operators of the two harmonic oscillator modes, respectivley, $\hat{c}$ is that of qC, E_J is the Josephson energy of qC, and $\phi_i (i = a, b, c)$ is the zero-point fluctuation of the phase associated with Alice, Bob, and qC, respectively.

The desired bilinear coupling is realized by supplying two drives whose detunings match that between Alice and Bob. The resulting interaction Hamiltonian can be written as [23]

$$\hat{H}_{\rm int}(t)/\hbar = g(t)(e^{i\varphi}\hat{a}\hat{b}^\dagger + e^{-i\varphi}\hat{a}^\dagger\hat{b}), \quad (2)$$

where φ is determined by the relative phases of the two drives, and the coupling coefficient is $g(t) = E_J\phi_a\phi_b\phi_c^2\xi_1(t)\xi_2(t) = \sqrt{\chi_{ac}\chi_{bc}}\xi_1(t)\xi_2(t)$ [23,27]. The strength of each drive $\xi_{1,2}$ is calibrated independently by measuring the Stark shift of the resonance frequency of qC. The dispersive couplings χ_{ac} and χ_{bc} are determined using standard number-splitting measurements [23]. This coupling between two harmonic modes has been shown [28] to transfer a quantum state from a memory to a propagating mode. Here, we engineer the same coupling but between two high-Q modes so that we can realize the unitary operation $\hat{U}(\theta) = \exp[-(i/\hbar)\int_0^T \hat{H}_{\rm int}(t)dt]$ while only virtually populating the excited levels of qC. We define $\theta = \int_0^T g(t)dt$ as the effective mixing angle [17] of the process. It is fully tunable by varying the duration of the drives. For $\theta = \pi/2 \pmod{\pi}$, the unitary performs a SWAP operation that exchanges the states of the two memories, while for $\theta = \pi/4 \pmod{\pi/2}$ it performs a 50:50 BS operation ($\hat{U}_{\rm BS}$).

We calibrate the strength of the engineered coupling by monitoring the dynamics of a single excitation under $\hat{U}(\theta)$. As shown in Fig. 2(a), we initialize the memories in $|1,0\rangle_{\rm AB}$ using numerically optimized pulses [29] while ensuring that qC remains in $|g\rangle$. We then apply the drives for a variable duration before measuring the joint population distribution in Alice and Bob using a photon-number selective π pulse on qC [30]. Using this method, we monitor the evolution of the single excitation as it coherently oscillates between the two memories ∼100 times faster than their photon loss rates. An example is shown in Fig. 2(b) at a coupling strength $g/2\pi = 34$ kHz. This corresponds to implementing a BS operation in $T_{\rm BS} = \pi/4g \approx 3.6$ μs, 2 orders of magnitude faster than the natural coupling ($\sim 1/\chi_{ab}$) between the two detuned memories

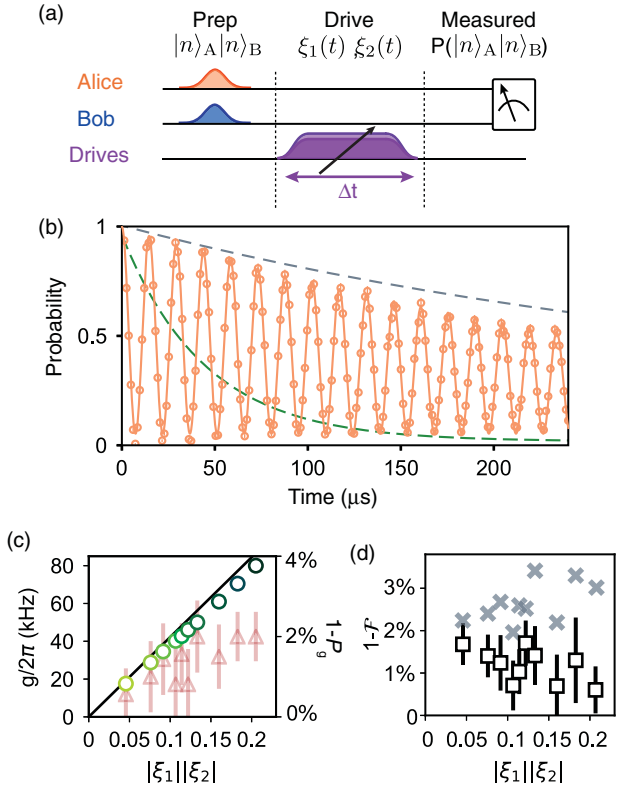

FIG. 2. Calibration of bilinear coupling. (a) General measurement protocol. After preparing the cavities in the desired initial state, we apply the drives for a variable amount of time before measuring the final joint memory state using a photon-number selective π pulse on qC. (b) Measured P_{10} (orange circles) with the engineered interaction at $|\xi_1||\xi_2| \approx 0.12$. Data are normalized by a constant scaling factor to calibrate out the state preparation and measurement errors [23]. Solid line shows fit to the functional form $P_{10} \propto e^{t/\tau_1}[1 + e^{t/\tau_\phi} \sin(2\pi t f)]$. Dashed lines are the intrinsic decays from $|1\rangle_A$ (gray) and relaxation of $|e\rangle$ (green) of qC. (c) Measured coupling strength $g/2\pi$ (green circles) as a function of the drive strength $|\xi_1||\xi_2|$. Data are consistent with the predicted behavior (black line) based on the fourth order cosine expansion, but deviate at higher drive powers. Measured excited state population of qC (red triangles), after a single BS operation. (d) Measured infidelity of a BS as defined by τ_{BS}/T_{BS} at different drive powers with (black squares) and without (gray crosses) postselecting on qC remaining in its ground state after the operation.

[23]. Thus, this ensures that the operation has a large on-off ratio.

We can assess the fidelity of the BS operation by analyzing the decoherence time associated with the evolution of a single excitation under $\hat{U}_\theta$. Two mechanisms could introduce nonidealities to the operation, namely, photon loss and dephasing. By summing the measured P_{10} and P_{01}, we obtain an envelope whose exponential decay gives the effective relaxation time τ_1. We can then divide P_{10} by this envelope to extract the dephasing time τ_ϕ using a decaying sinusoidal fit. For the data shown in Fig. 2(b), we extract an effective $\tau_1 \simeq 400\ \mu s$ and $\tau_\phi \simeq 800\ \mu s$ at $|\xi_1||\xi_2| \approx 0.12$. Both are consistent with independent measurements of the coherence times of Alice and Bob. Combining these, we infer an effective decoherence time $1/\tau_{BS} = 1/2\tau_1 + 1/\tau_\phi \approx 400\ \mu s$ for the operation with an infidelity of $\sim 1\%$ obtained by comparing this to the time required to implement $\hat{U}_{BS}$ at this drive power.

We then characterize the coupling strength and the fidelity of the BS at different drive powers. We show in Fig. 2(c) that g scales linearly with $|\xi_1||\xi_2|$ at low powers, consistent with the predictions from the fourth order expansion of Eq. (1). However, it deviates from this simple model when the drives are stronger, which can be explained by a perturbation theory treatment [23]. Naively, one might think that the decoherence would contribute less to the infidelity as the operation speeds up. However, as g increases, so does the participation of the qC excited levels, which are measured independently after each BS. We observe that the probability of qC departing from its ground state $1 - P_g$ increases from 0.6% to 2% as we increase the drive strengths. The effect of this is twofold: an apparent reduction in the readout contrast

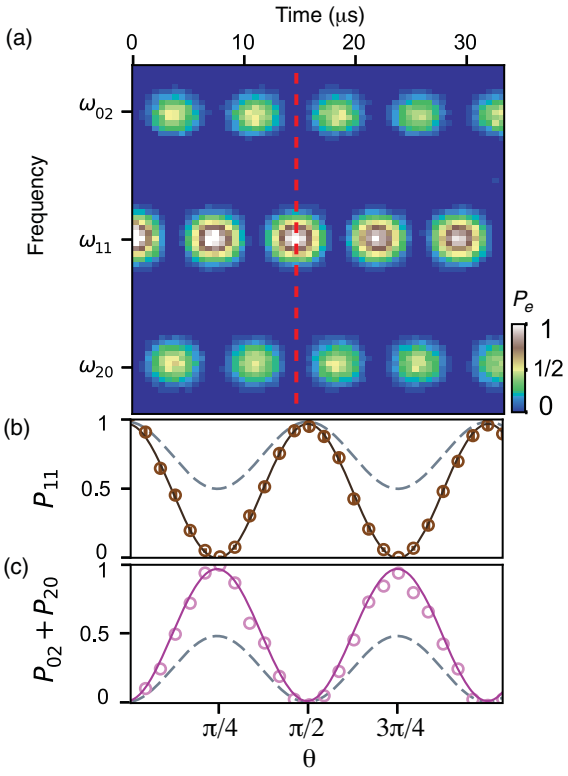

FIG. 3. HOM interference between Alice and Bob. (a) Data show the joint population as the initial state $|1,1\rangle_{AB}$ evolves under $\hat{U}_\theta$. We observe out-of-phase oscillations between P_{11} and an equal superposition of $|0,2\rangle_{AB}$ and $|2,0\rangle_{AB}$. (b),(c) 1D cuts to show the behavior of P_{11} (brown) and $P_{02} + P_{20}$ (magenta) up to $\sim 15\ \mu s$ (red dashed line). A simulation of two indistinguishable photons is shown in solid lines and that of two distinguishable photons is shown in dashed gray lines.

as well as faster decoherence during $\hat{U}_{\mathrm{BS}}$. The former can be mitigated by performing postselection: data are discarded if qC does not remain in $|g\rangle$ after the operation. This ensures that qC is a faithful meter for the joint photon population of Alice and Bob. We attribute the degradation of coherence to the greater participation of qC. This causes the system to inherit less favorable coherence times during $\hat{U}_{\mathrm{BS}}$ [23]. Combining the faster operations and the penalty due to increased qC participation, the overall infidelity ends up roughly constant over different drive powers, as shown in Fig. 2(d). For subsequent experiments, we operate at $|\xi_1||\xi_2| \simeq 0.1$, where the drives do not introduce measurable nonidealities on top of the intrinsic decoherence of the system.

III. INTERFERENCE BETWEEN TWO MICROWAVE QUANTUM MEMORIES

The quality of the BS operation can also be characterized by the contrast of HOM interference, which is the hallmark of interference between two indistinguishable bosonic modes. We demonstrate that this behavior can be observed between two photons at different frequencies via the engineered frequency-converting coupling, similar to the results described in Ref. [31]. We start by preparing $|1,1\rangle_{\mathrm{AB}}$ and monitor the joint population of Alice and Bob after applying the drive tones. The photon-number distribution of Alice and Bob is probed by performing a photon-number selective π pulse on qC at different frequencies. The population of a particular joint photon-number state $|n,m\rangle_{\mathrm{AB}}$ is given by the probability of exciting qC at $\omega_{nm} = \omega_c - n\chi_{ac} - m\chi_{bc}$, as shown in Fig. 3(a). Two important observations can be made from this measurement.

First, the data indicate that the engineered BS operation indeed allows two detuned photons to behave as indistinguishable particles. This is shown by near complete destruction of the $|1,1\rangle_{\mathrm{AB}}$ signal after the BS. At this point, we also measure an equal probability of finding the system in states $|2,0\rangle_{\mathrm{AB}}$ and $|0,2\rangle_{\mathrm{AB}}$. This interference is an intrinsically quantum mechanical phenomena. It typically relies on the two initial photons being fully indistinguishable such that the probability amplitudes of $|1,1\rangle_{\mathrm{AB}}$ after the BS destructively interfere. When two photons are distinguishable, the classical probability distribution is observed and the measured P_{11} always remain above 0.5. In this case, since the two cavity modes are far detuned from each other, the initial excitations are completely distinct. The observation of quantum interference depends crucially on the frequency-converting coupling that can fully compensate for the energy difference between the two initial photons. Therefore, the measured HOM contrast of $98 \pm 1\%$ is a direct indication of the quality of the engineered BS operation.

Second, we know that the BS operation preserves the phase coherence of the superposition states. This is demonstrated by the near unit probability of $|1,1\rangle_{\mathrm{AB}}$ after the second BS with full extinction of $|2,0\rangle_{\mathrm{AB}}$ and $|0,2\rangle_{\mathrm{AB}}$. Thus, we infer that the system is indeed in a coherent superposition of $|2,0\rangle_{\mathrm{AB}}$ and $|0,2\rangle_{\mathrm{AB}}$ after the first BS because a statistically mixed state would not allow the full constructive interference of $|1,1\rangle_{\mathrm{AB}}$. Consequently, it would lead to a reduction of the P_{11} contrast.

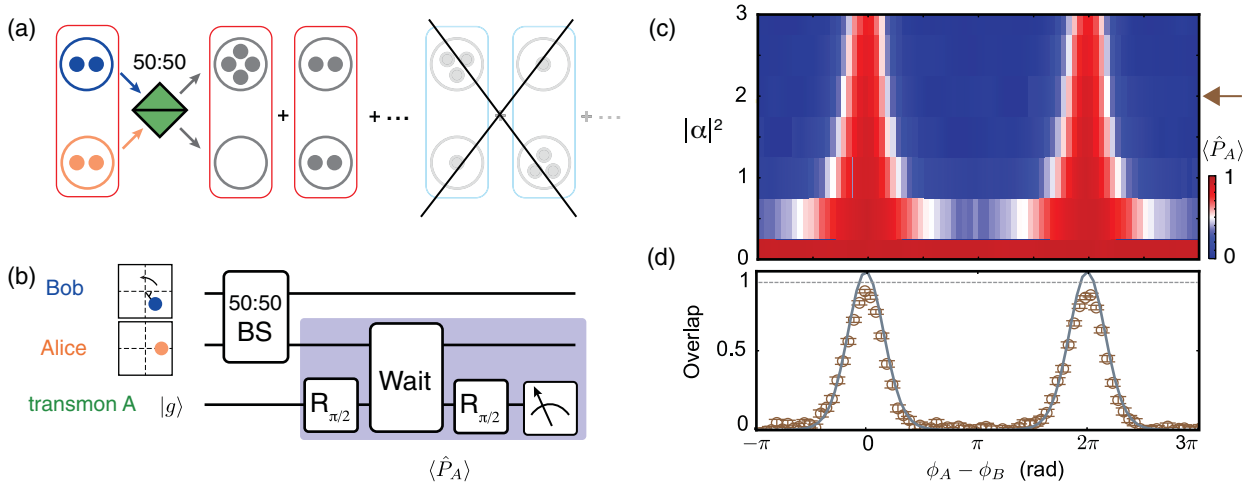

FIG. 4. Measurement of quantum state overlap. (a) When two identical bosonic systems interfere at a 50:50 BS, only even photon-number outcomes are allowed due to the full destructive interference of the odd distributions. This allows us to infer the state overlap $\mathrm{Tr}(\rho_A \rho_B)$ from photon-number parity measurement of one of the output ports. (b) The experimental protocol for implementing the overlap measurement between Alice and Bob. (c) Measurement of overlap between $|\psi\rangle_A = e^{i\phi_A}|\alpha\rangle$ and $|\psi\rangle_B = e^{i\phi_B}|\alpha\rangle$ as a function of the relative displacement angle $(\phi_A - \phi_B)$ and amplitude α. Maximum overlap for each displacement is measured when $\phi_B = \phi_A$ (mod 2π). (d) 1D cut at displacement of $|\alpha|^2 \approx 2$. Data are shown in brown circles, which shows good agreement with the overlap determined by full Wigner tomography of each mode, shown in solid gray line. The dashed gray line indicates the predicated peak contrast after taking into account self-Kerr and the decoherence of the cavities.

The HOM experiment reveals an intrinsic property of bosonic systems: when two identical quantum states interfere through a 50:50 BS, the photon-number parity of the output ports is always even because the odd outcomes interfere destructively, as illustrated in Fig. 4(a). In fact, it has been proven that the average parity measured on one of the output ports after a BS is a direct probe of the overlap between the two initial states; i.e., $\langle \hat{P}_A \rangle = \mathrm{Tr}(\rho_A \rho_B)$ [7,22,32,33]. This establishes a mapping between the state overlap and a single observable that is the photon-number parity of one of the output modes regardless of the input states.

As a demonstration, we perform direct overlap measurement between two coherent states $|\psi\rangle_A = e^{i\phi_A}|\alpha\rangle$ and $|\psi\rangle_B = e^{i\phi_B}|\alpha\rangle$ using a single BS and robust parity measurement enabled by the natural dispersive coupling between qA and Alice in our cQED system [34,35]. The experimental sequence is outlined in Fig. 4(b), where ϕ_A is fixed and the parity of Alice is measured as a function of ϕ_B for variable displacement amplitude α in both cavities. As expected, the maximum overlap is measured when $\phi_A = \phi_B (\mathrm{mod}\ 2\pi)$, and as the displacement increases, the measured $\langle \hat{P}_A \rangle$ becomes more sharply peaked. This is in good agreement with the ideal $\mathrm{Tr}(\rho_A \rho_B)$ calculated using simulated full Wigner functions of each mode. We do observe a reduction in the overall contrast at higher photon numbers which can be accounted for by known imperfections of the parity measurement and the BS operation [23].

In addition to the engineered BS operation, we can also implement on-demand DPS to Alice via its natural dispersive coupling (χ_1) to qA. This is governed by the unitary $\hat{U}_{\mathrm{DPS}}(\phi) = |g\rangle\langle g| \otimes \hat{I} + |e\rangle\langle e| \otimes e^{i\phi \hat{a}^\dagger \hat{a}}$, where $\phi = \chi_1 t$. This implementation has two major advantages. It is fully programmable: the resulting differential phase, $\phi \in [0, 2\pi]$, is simply controlled by the evolution time t, which can be tuned on the fly. Furthermore, it is photon-number independent: $\hat{U}_{\mathrm{DPS}}$ allows us to impart the same phase to each individual photon in Alice. Therefore, it is naturally compatible with more complex interference experiments involving multiphoton states.

Combining the BS and DPS capabilities, we can construct cascaded MZ interferometers and program them to perform different interference experiments on the fly [Fig. 5(a)]. As a simple example, we initialize the system in $|1,1\rangle_{\mathrm{AB}}$. After a single BS, the system reaches the superposition state $|\Psi\rangle = (1/\sqrt{2})(|0,2\rangle_{\mathrm{AB}} + e^{i\varphi}|2,0\rangle_{\mathrm{AB}})$. Subsequently, we can impart a phase on Alice by exciting qA for a time $\pi/\chi_1 \sim 500$ ns. This operation changes the relative phase between Alice and Bob, leaving the system in the state $|\Phi\rangle = (1/\sqrt{2})(|0,2\rangle_{\mathrm{AB}} + e^{i(\varphi+\pi)}|2,0\rangle_{\mathrm{AB}})$. This is now a "dark state" of $\hat{U}_{\mathrm{BS}}$ because the probability amplitudes of $|1,1\rangle_{\mathrm{AB}}$ always interfere destructively, forcing the system to remain in $|\Phi\rangle$ through all subsequent beam splitters. We then bring the system back to $|\Psi\rangle$ and recover the HOM-type interference by implementing a second DPS of π on Alice. The reduced contrast in the revival of $|1,1\rangle_{\mathrm{AB}}$ can be attributed to the nonidealities due to both the self-Kerr and the dephasing of the memory modes during the evolution in the dark state.

Such cascaded interferometers, similar to optical implementations, such as in Ref. [36], offer a versatile and scalable scheme to study complex interference phenomena and boson statistics. In particular, all components in our implementation are by design compatible with multiphoton states. Combining this with our ability to prepare complex bosonic states and efficiently probe their statistics using the transmon ancilla, we can easily extend such cascaded interferometers to investigate the interference between a larger number of excitations. A simple demonstration is shown in Fig. S5 of the Supplemental Material, where two memories initialized in a state

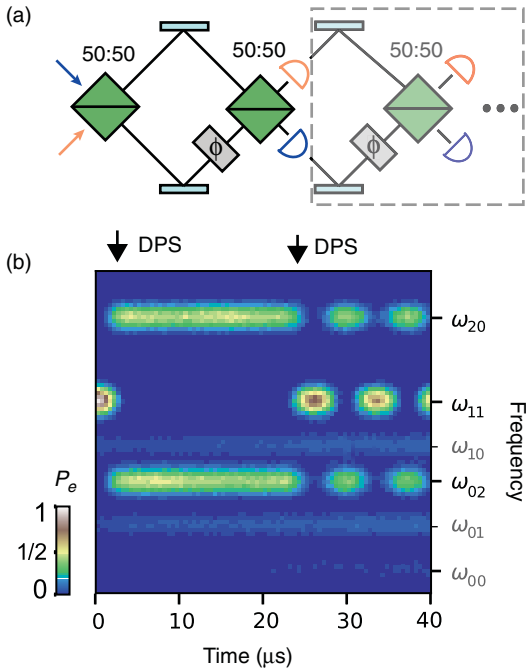

FIG. 5. Cascaded Mach-Zehnder interferometers composed of BS, DPS, and photon counters. (a) Conceptual implementation of programmable cascaded Mach-Zehnder (MZ) interferometers between two detuned modes. We can measure the state of the system after each operation and implement DPS on demand. (b) Evolution of $|1,1\rangle_{\mathrm{AB}}$ in cascaded microwave MZ interferometers, measured by sweeping the frequency of a photon-number selective π pulse on qC while varying the duration of the drive tones. After the first BS, a coherent superposition of $|0,2\rangle_{\mathrm{AB}}$ and $|2,0\rangle_{\mathrm{AB}}$ ($|\Psi\rangle$) is created. Subsequently, we impart a differential phase $\phi = \pi$, which leaves the system in $|\Phi\rangle$ and causes $|1,1\rangle_{\mathrm{AB}}$ to destructively interfere through the subsequent BSs. We then introduce another differential phase π such that the system is brought back to the original superposition $|\Psi\rangle$, which refocuses to $|1,1\rangle_{\mathrm{AB}}$ at the subsequent BS, as in standard HOM interference.

containing three excitations interfere through a series of engineered BS [23].

IV. CONCLUSION

In conclusion, we engineer a robust BS operation between bosonic quantum memories in a fixed-frequency cQED architecture. With this, we demonstrate high-contrast HOM interference between two memories at different frequencies. Furthermore, we combine this coupling with single-cavity phase control and photon-number parity measurement to implement efficient overlap measurements and on-demand manipulation of the signature of two-photon interference. Taking advantage of the tunability of the BS and our ability to implement DPS on the fly, we construct highly programmable cascaded interferometers capable of manipulating interference statistics on demand. Our implementation can be directly extended to higher photon numbers to study more complex interference between multiphoton states [23]. The robust BS and DPS operations demonstrated in this work form an essential tool set for implementing gates between logical qubits encoded in superconducting cavities [37–39]. Additionally, our results provide the essential components required for implementing linear optical quantum computing protocols [11,40] in the cQED framework.

ACKNOWLEDGMENTS

We thank M. H. Devoret for helpful discussions, N. Frattini, K. Sliwa, M. J. Hatridge, and A. Narla for providing the Josephson Parametric Converters (JPCs), and N. Ofek and P. Reinhold for providing the logic and control interface for the field programmable gate array used in this experiment. This research was supported by the U.S. Army Research Office (W911NF-14-1-0011). Y. Y. G. was supported by an A*STAR NSS Fellowship; B. J. L. is supported by Yale QIMP Fellowship; S. M. G. is supported by the National Science Foundation (DMR-1609326); L. J. is supported by the Alfred P. Sloan Foundation (BR 2013-049) and the Packard Foundation (2013-39273). Facilities use was supported by the Yale Institute for Nanoscience and Quantum Engineering (YINQE), the Yale SEAS clean room, and the National Science Foundation (MRSECDMR-1119826).

[1] C. K. Hong, Z. Y. Ou, and L. Mandel, *Measurement of Subpicosecond Time Intervals between Two Photons by Interference*, Phys. Rev. Lett. **59**, 2044 (1987).

[2] A. M. Kaufman, B. J. Lester, C. M. Reynolds, M. L. Wall, M. Foss-Feig, K. R. Hazzard, A. M. Rey, and C. A. Regal, *Two-Particle Quantum Interference in Tunnel-Coupled Optical Tweezers*, Science **345**, 306 (2014).

[3] E. Bocquillon, V. Freulon, J. M. Berroir, P. Degiovanni, B. Placais, A. Cavanna, Y. Jin, and G. Feve, *Coherence and Indistinguishability of Single Electrons Emitted by Independent Sources*, Science **339**, 1054 (2013).

[4] R. Lopes, A. Imanaliev, A. Aspect, M. Cheneau, D. Boiron, and C. I. Westbrook, *Atomic Hong-Ou-Mandel Experiment*, Nature (London) **520**, 66 (2015).

[5] K. Toyoda, R. Hiji, A. Noguchi, and S. Urabe, *Hong-Ou-Mandel Interference of Two Phonons in Trapped Ions*, Nature (London) **527**, 74 (2015).

[6] M. C. Tichy, *Interference of Identical Particles from Entanglement to Boson-Sampling*, J. Phys. B **47**, 103001 (2014).

[7] R. Islam, R. Ma, P. M. Preiss, M. E. Tai, A. Lukin, M. Rispoli, and M. Greiner, *Measuring Entanglement Entropy in a Quantum Many-Body System*, Nature (London) **528**, 77 (2015).

[8] A. Aspect, *Bell's Inequality Test: More Ideal Than Ever*, Nature (London) **398**, 189 (1999).

[9] H. J. Kimble, Y. Levin, A. B. Matsko, K. S. Thorne, and S. P. Vyatchanin, *Conversion of Conventional Gravitational-Wave Interferometers into Quantum Nondemolition Interferometers by Modifying Their Input and/or Output Optics*, Phys. Rev. D **65**, 022002 (2001).

[10] D. Leibfried, B. DeMarco, V. Meyer, M. Rowe, A. Ben-Kish, J. Britton, W. M. Itano, B. Jelenkovic, C. Langer, T. Rosenband, and D. J. Wineland, *Trapped-Ion Quantum Simulator: Experimental Application to Nonlinear Interferometers*, Phys. Rev. Lett. **89**, 247901 (2002).

[11] E. Knill, R. Laflamme, and G. J. Milburn, *A Scheme for Efficient Quantum Computation with Linear Optics*, Nature (London) **409**, 46 (2001).

[12] P. Kok, W. J. Munro, K. Nemoto, T. C. Ralph, J. P. Dowling, and G. J. Milburn, *Linear Optical Quantum Computing with Photonic Qubits*, Rev. Mod. Phys. **79**, 135 (2007).

[13] B. Peropadre, G. G. Guerreschi, J. Huh, and A. Aspuru-Guzik, *Proposal for Microwave Boson Sampling*, Phys. Rev. Lett. **117**, 140505 (2016).

[14] M. Hofheinz, E. M. Weig, M. Ansmann, R. C. Bialczak, E. Lucero, M. Neeley, A. D. O'Connell, H. Wang, J. M. Martinis, and A. N. Cleland, *Generation of Fock States in a Superconducting Quantum Circuit*, Nature (London) **454**, 310 (2008).

[15] R. W. Heeres, B. Vlastakis, E. Holland, S. Krastanov, V. V. Albert, L. Frunzio, L. Jiang, and R. J. Schoelkopf, *Cavity State Manipulation Using Photon-Number Selective Phase Gates*, Phys. Rev. Lett. **115**, 137002 (2015).

[16] C. Lang, C. Eichler, L. Steffen, J. M. Fink, M. J. Woolley, A. Blais, and A. Wallraff, *Correlations, Indistinguishability and Entanglement in Hong-Ou-Mandel Experiments at Microwave Frequencies*, Nat. Phys. **9**, 345 (2013).

[17] F. Nguyen, E. Zakka-Bajjani, R. W. Simmonds, and J. Aumentado, *Quantum Interference between Two Single Photons of Different Microwave Frequencies*, Phys. Rev. Lett. **108**, 163602 (2012).

[18] M. Mariantoni, H. Wang, R. C. Bialczak, M. Lenander, E Lucero, M. Neeley, A. D. OConnell, D. Sank, M. Weides, J. Wenner, T. Yamamoto, Y. Yin, J. Zhao, J. M. Martinis, and A. N. Cleland, *Photon Shell Game in Three-Resonator Circuit Quantum Electrodynamics*, Nat. Phys. **7**, 287 (2011).

[19] M. Pierre, S. R. Sathyamoorthy, I. Svensson, G. Johansson, and P. Delsing, *Resonant and Off-Resonant Microwave Signal Manipulations in Coupled Superconducting Resonators*, arXiv:1802.09034.

[20] M. Reagor, H. Paik, G. Catelani, L. Sun, C. Axline, E. Holland, I. M. Pop, N. A. Masluk, T. Brecht, L. Frunzio, M. H. Devoret, L. Glazman, and R. J. Schoelkopf, *Reaching 10 ms Single Photon Lifetimes for Superconducting Aluminum Cavities*, Appl. Phys. Lett. **102**, 192604 (2013).

[21] A. Romanenko and D. I. Schuster, *Understanding Quality Factor Degradation in Superconducting Niobium Cavities at Low Microwave Field Amplitudes*, Phys. Rev. Lett. **119**, 264801 (2017).

[22] R. Filip, *Overlap and Entanglement-Witness Measurements*, Phys. Rev. A **65**, 062320 (2002).

[23] See Supplemental Materials at http://link.aps.org/supplemental/10.1103/PhysRevX.8.021073 for information about the device parameters, detailed data analysis, and extended data.

[24] C. Wang, Y. Y. Gao, P. Reinhold, R. W. Heeres, N. Ofek, K. Chou, C. Axline, M. Reagor, J. Blumoff, K. M. Sliwa, L. Frunzio, S. M. Girvin, L. Jiang, M. Mirrahimi, M. H. Devoret, and R. J. Schoelkopf, *A Schrodinger Cat Living in Two Boxes*, Science **352**, 1087 (2016).

[25] S. E. Nigg, H. Paik, B. Vlastakis, G. Kirchmair, S. Shankar, L. Frunzio, M. H. Devoret, R. J. Schoelkopf, and S. M. Girvin, *Black-Box Superconducting Circuit Quantization*, Phys. Rev. Lett. **108**, 240502 (2012).

[26] Z. Leghtas, S. Touzard, I. M. Pop, A. Kou, B. Vlastakis, A. Petrenko, K. M. Sliwa, A. Narla, S. Shankar, M. J. Hatridge, M. Reagor, L. Frunzio, R. J. Schoelkopf, M. Mirrahimi, and M. H. Devoret, *Quantum Engineering. Confining the State of Light to a Quantum Manifold by Engineered Two-Photon Loss*, Science **347**, 853 (2015).

[27] Y. Zhang and S. M. Girvin (to be published).

[28] W. Pfaff, C. J. Axline, L. D. Burkhart, U. Vool, P. Reinhold, L. Frunzio, L. Jiang, M. H. Devoret, and R. J. Schoelkopf, *Controlled Release of Multiphoton Quantum States from a Microwave Cavity Memory*, Nat. Phys. **13**, 882 (2017).

[29] R. W. Heeres, P. Reinhold, N. Ofek, L. Frunzio, L. Jiang, M. H. Devoret, and R. J. Schoelkopf, *Implementing a Universal Gate Set on a Logical Qubit Encoded in an Oscillator*, Nat. Commun. **8**, 94 (2017).

[30] D. I. Schuster, A. A. Houck, J. A. Schreier, A. Wallraff, J. M. Gambetta, A. Blais, L. Frunzio, J. Majer, B. Johnson, M. H. Devoret, S. M. Girvin, and R. J. Schoelkopf, *Resolving Photon Number States in a Superconducting Circuit*, Nature (London) **445**, 515 (2007).

[31] T. Kobayashi, R. Ikuta, S. Yasui, S. Miki, T. Yamashita, H. Terai, T. Yamamoto, M. Koashi, and N. Imoto, *Frequency-Domain Hong-Ou-Mandel Interference*, Nat. Photonics **10**, 441 (2016).

[32] A. J. Daley, H. Pichler, J. Schachenmayer, and P. Zoller, *Measuring Entanglement Growth in Quench Dynamics of Bosons in an Optical Lattice*, Phys. Rev. Lett. **109**, 020505 (2012).

[33] A. K. Ekert, C. M. Alves, D. K. L. Oi, M. Horodecki, P. Horodecki, and L. C. Kwek, *Direct Estimations of Linear and Nonlinear Functionals of a Quantum State*, Phys. Rev. Lett. **88**, 217901 (2002).

[34] P. Bertet, A. Auffeves, P. Maioli, S. Osnaghi, T. Meunier, M. Brune, J. M. Raimond, and S. Haroche, *Direct Measurement of the Wigner Function of a One-Photon Fock State in a Cavity*, Phys. Rev. Lett. **89**, 200402 (2002).

[35] L. Sun, A. Petrenko, Z. Leghtas, B. Vlastakis, G. Kirchmair, K. M. Sliwa, A. Narla, M. Hatridge, S. Shankar, J. Blumoff, L. Frunzio, M. Mirrahimi, M. H. Devoret, and R. J. Schoelkopf, *Tracking Photon Jumps with Repeated Quantum Non-Demolition Parity Measurements*, Nature (London) **511**, 444 (2014).

[36] A. Crespi, R. Osellame, R. Ramponi, D. J. Brod, E. F. Galvo, N. Spagnolo, C. Vitelli, E. Maiorino, P. Mataloni, and F. Sciarrino, *Integrated Multimode Interferometers with Arbitrary Designs for Photonic Boson Sampling*, Nat. Photonics **7**, 545 (2013).

[37] M. Mirrahimi, Z. Leghtas, V. V. Albert, S. Touzard, R. J. Schoelkopf, L. Jiang, and M. H. Devoret, *Dynamically Protected Cat-Qubits: A New Paradigm for Universal Quantum Computation*, New J. Phys. **16**, 045014 (2014).

[38] H. K. Lau and M. B. Plenio, *Universal Quantum Computing with Arbitrary Continuous-Variable Encoding*, Phys. Rev. Lett. **117**, 100501 (2016).

[39] S. Lloyd, M. Mohseni, and P. Rebentrost, *Quantum Principal Component Analysis*, Nat. Phys. **10**, 631 (2014).

[40] L. Chirolli, G. Burkard, S. Kumar, and D. P. DiVincenzo, *Superconducting Resonators as Beam Splitters for Linear-Optics Quantum Computation*, Phys. Rev. Lett. **104**, 230502 (2010).